Inorganic Chemistry

Article

pubs.acs.org/IC

Highly Sensitive and Selective Rhodamine-Based "Off–On" Reversible Chemosensor for Tin (Sn^{4+}) and Imaging in Living Cells

Ajit Kumar Mahapatra,*[,†] Saikat Kumar Manna,[†] Debasish Mandal,[§] and Chitrangada Das Mukhopadhyay[‡]

[†]Department of Chemistry and [‡]Centre for Healthcare Science & Technology, Bengal Engineering and Science University, Shibpur, Howrah—711103, India

[§]Department of Spectroscopy, Indian Association for The Cultivation of Science, Jadavpur, Kolkata—700032, India

Supporting Information

ABSTRACT: A structurally characterized new oxo-chromene functionalized rhodamine derivative **L1** exhibits high selectivity toward Sn^{4+} by forming a 1:1 complex, among other biologically important metal ions, as studied by fluorescence, absorption, and HRMS spectroscopy. Complexing with Sn^{4+} triggers the formation of a highly fluorescent ring-open form which is pink in color. The sensor shows extremely high fluorescence enhancement upon complexation with Sn^{4+}, and it can be used as a "naked-eye" sensor. DFT computational studies carried out in mimicking the formation of a 1:1 complex between **L1** and Sn^{4+} resulted in a nearly planar pentacoordinate Sn(IV) complex. Studies reveal that the *in situ* prepared **L1**–Sn complex is selectively and fully reversible in presence of sulfide anions. Further, confocal microscopic studies confirmed that the receptor shows *in vitro* detection of Sn^{4+} ions in RAW cells.

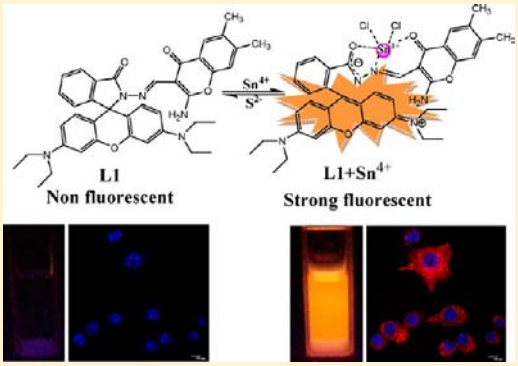

INTRODUCTION

The design and development of optical sensors for selective recognition and sensing of environmentally and biologically important metal ions is an important and contemporary research area. In this regard, metal ions that are known to have harmful effects on living organisms or the environment are generally more common as target metal ions for such studies.[1] Among the different metal ions, tetravalent tin, Sn^{4+}, is an important trace mineral for human and animal biology as it is involved in several biochemical processes at the cellular level.[2a] Tin deficiency can increase the risk factors associated with poor growth, hearing loss, and cancer prevention. Some severe immunotoxic and neurotoxic effects of tin have been reported, with symptoms mostly associated to gastrointestinal complaints such as nausea, abdominal pain, and vomiting.[2b] In addition, tin compound is a known environmental pollutant due to its widespread use as chemical reagent, agricultural, chemical weapon, and industrial activities.[3] Therefore, great importance is attached to developing selective chemosensors for tin. In this aspect, fluorogenic methods with suitable probes are preferable approaches for the measurement of these analytes because fluorimetry is rapidly performed, is nondestructive, is highly sensitive, is suitable for high-throughput screening applications, and can afford real information on the localization and quantity of the targets of interest. In recent years, significant emphasis has been placed on the development of new, highly selective fluorescent chemosensors of different architectures for metal cations because of their potential applications in biochemistry and environmental research.[4]

It is familiar that rhodamine B is a classic fluorescent dye and its derivatives (RhB) are extensively used as a fluorescent chemosensor because of their excellent photophysical properties, such as high extinction coefficients (>75 000 cm^{-1} M^{-1}), excellent quantum yields,[5] great photostability,[6] and relatively long emission wavelengths in the visible region.[7] In addition, the equilibrium between the nonfluorescent spirocyclic form and the highly fluorescent ring-open form provides a better model for the development of turn-on sensors. So, rhodamine B is widely used as a fluorescent probe for the detection of cysteine[8] and metal ions,[9] including Cu^{2+},[10] Cr^{3+},[11] Fe^{3+},[12] Hg^{2+},[13] Pb^{2+},[14] Zn^{2+},[15] Au^{3+},[16] Ba^{2+},[17] and Al^{3+},[18] due to the ring-opening reaction of rhodamine.

With the above-mentioned criteria in mind, herein we introduced oxo-benzopyran or oxo-chromene moiety to rhodamine, and we synthesized a chemosensor, **L1** (Scheme 1),[19] which can give highly selective and rapid responses to Sn^{4+} in living cells. As far as we are aware, **L1** is the first oxo-chromene based Sn^{4+} sensor on rhodamine derivative. The structure of chemosensor **L1** was verified by ^{1}H NMR, ^{13}C NMR, mass spectra, and elemental analyses (Figures S1–S3, Supporting Information). Our sensor shows extremely high sensitivity compared to the recently developed[9d] Sn^{4+} sensors attributed to the very high association constants for the binding of Sn^{4+}.

Received: March 21, 2013
Published: September 25, 2013

Scheme 1. Synthetic Scheme for Compound L1

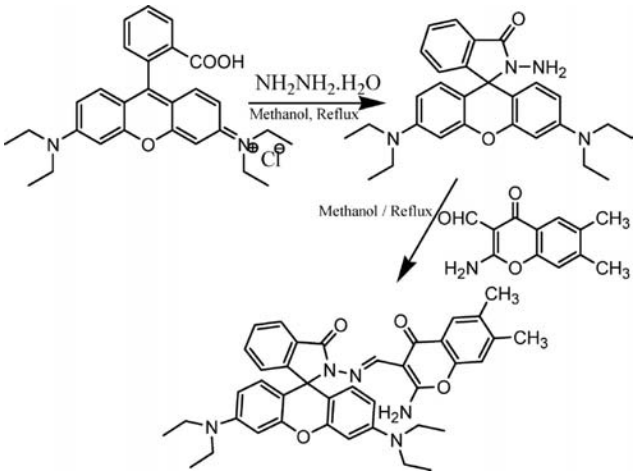

EXPERIMENTAL SECTION

General Information and Materials. All the solvents were of analytic grade. All cationic compounds such as perchlorate of Hg^{2+}, Cu^{2+}, Cd^{2+}, Fe^{2+}, Co^{2+}, Ni^{2+}, Mn^{2+}, Zn^{2+}, Mg^{2+}, nitrate of Ag^{+}, chlorides of Cr^{3+}, Ca^{2+}, Al^{3+}, Fe^{3+}, Pb^{2+}, and $SnCl_4{\cdot}5H_2O$ were purchased from Sigma–Aldrich Chemical Co., stored in a desiccators under vacuum containing self-indicating silica, and used without any further purification. Solvents were dried according to standard procedures. Unless stated otherwise, commercial grade chemicals were used without further purification. Elix Millipore water was used throughout all experiments. All reactions were magnetically stirred and monitored by thin-layer chromatography (TLC) using Spectrochem GF254 silica gel coated plates. Column chromatography was performed with activated neutral aluminum oxide. FTIR spectra were recorded as KBr pellets using a JASCO FTIR spectrometer (model FTIR-460 plus). The ^{1}H NMR spectra were recorded on Bruker 400 MHz spectrometer. Mass spectra were carried out using a Waters QTOF Micro YA 263 mass spectrometer. The ^{1}H NMR chemical shift values are expressed in ppm (δ) relative to $CHCl_3$ (δ = 7.26 ppm). UV–vis and fluorescence spectra measurements were performed on a JASCO V530 and a Photon Technology International (PTI-LPS-220B) spectrofluorimeter, respectively. The following abbreviations are used to describe spin multiplicities in ^{1}H NMR spectra: s = singlet; d = doublet; t = triplet; m = multiplet. Elemental analyses were performed with a Perkin-Elmer 2400 elemental analyzer.

Synthesis of L1. Rhodamine B hydrazide (0.40 g, 0.88 mmol) and 2-amino-6,7-dimethyl-4-oxo-4*H*-1-benzopyran-3-carbaldehyde (0.19 g, 0.88 mmol) were dissolved in 20 mL of dry methanol, and the resulting solution was refluxed for 12 h. The solvent was then evaporated *in vacuo*, and the residue was extracted with water/dichloromethane. The organic layer was dried over sodium sulfate. After filtration and evaporation of the solvent *in vacuo*, the residue was chromatographed on silica gel with hexane/ethyl acetate (7:3, v/v) as eluent to give **L1** as a white solid in 85% yield. Mp > 250 °C. ^{1}H NMR (d_6-DMSO, 400 MHz) δ (ppm): 9.26 (1H, s, CH=N), 7.88 (1H, d, J = 8.00 Hz), 7.56–7.59 (2H, m), 7.21 (1H, s), 7.13 (1H, s), 7.09(1H, d, J = 6.8 Hz), 6.32–6.39 (6H, m), 4.03 (2H, s), 3.30 (q, 8H, J = 6.9 Hz, NCH_2CH$_3$), 2.29 (3H, s), 2.24 (3H, s), 1.07 (12H, t, J = 6.9 Hz, NCH$_2$$CH_3$). ^{13}C NMR ($CDCl_3$, 400 MHz) δ (ppm): 14.11, 19.15, 20.19, 22.67, 29.34, 29.68, 31.91, 46.11, 60.39, 96.68, 114.19, 116.70, 117.08, 119.77, 123.62, 123.74, 125.80, 126.06, 12 8.82, 133.22, 133.70, 142.79, 151.33, 162.41, 174.79, 189.85. TOF MS ES+, m/z = 656.06 $[M + 1]^+$, calcd for $C_{40}H_{41}N_5O_4$ = 655.78. Anal. Calcd for $C_{40}H_{41}N_5O_4$: C, 73.26; H, 6.30; N, 10.68. Found: C, 73.17; H, 6.27; N, 10.71.

UV–Vis and Fluorescence Spectral Studies. A stock solution of the probe **L1** (4.0×10^{-5} M) was prepared in CH_3OH/H_2O (4:1, v/v). Solutions of 2.0×10^{-4} M salts of the respective cation were prepared in Millipore water. All experiments were carried out in CH_3OH/H_2O solution (CH_3OH/H_2O = 4:1, v/v, 10 μM HEPES buffer, pH = 7.4). In titration experiments, each time a 4×10^{-5} M solution of **L1** was filled in a quartz optical cell of 1 cm optical path length, and the ion stock solutions were added into the quartz optical cell gradually by using a micropipet. Spectral data were recorded at 1 min after the addition of the ions. In selectivity experiments, the test samples were prepared by placing appropriate amounts of the anions/cations stock into 2 mL of solution of **L1** (4×10^{-5} M). For fluorescence measurements, excitation was provided at 555 nm, and emission was collected from 560 to 700 nm.

Evaluation of the Association Constant for the Formation of L1·Sn^{4+}. Receptor **L1** with an effective concentration of 4×10^{-5} M in CH_3OH/H_2O solution (CH_3OH/H_2O = 4:1, v/v, 10 μM HEPES buffer, pH = 7.4) was used for the emission titration studies with a Sn^{4+} solution. A stock solution of $SnCl_4{\cdot}5H_2O$, having a concentration of 2×10^{-4} M in an aqueous HEPES buffer (3:2, v/v; pH 7.4) solution, was used.

Calculations for the Binding Constants Using Spectrophotometric Titration Data. The association constant and stoichiometry for the formation of the respective complexes were evaluated using the Benesi–Hildebrand (B–H) plot (eq 1).[20]

$$1/(I - I_0) = 1/K(I_{max} - I_0)[M^{n+}] + 1/(I_{max} - I_0) \quad (1)$$

Here I_0, I_{max}, and I represent the emission intensity of free **L1**, the maximum emission intensity observed in the presence of added metal ion at 580 nm for Sn^{4+} (λ_{ext} = 555 nm), and the emission intensity at a certain concentration of the metal ion added, respectively. Binding stoichiometries for the respective complex formations were also confirmed from Job's plot.

Finding the Detection Limit. The detection limit was calculated on the basis of the fluorescence titration (Supporting Information). The fluorescence emission spectrum of **L1** was measured 14 times, and the standard deviation of blank measurement was achieved. To gain the slope, the ratio of the fluorescence intensity at 580 nm was plotted as a concentration of Sn^{4+}. So the detection limit was calculated with the following equation[10b,21]

$$\text{detection limit} = 3Sb1/S \quad (2)$$

where Sbl is the standard deviation of blank measurement and S is the slope of the calibration curve.

Cell Culture. Frozen human colorectal carcinoma cell line HCT 116 (ATCC: CCL-247) was obtained from the American Type Culture Collection (Rockville, MD) and maintained in Dulbecco's modified Eagle's medium (DMEM, Sigma Chemical Co., St. Louis, MO) supplemented with 10% fetal bovine serum (Invitrogen), penicillin (100 μg/mL), and streptomycin (100 μg/mL). The RAW 264.7 macrophages were obtained from NCCS, Pune, India, and maintained in DMEM containing 10% (v/v) fetal calf serum and antibiotics in a CO_2 incubator. Cells were initially propagated in 25 cm^2 tissue culture flask in an atmosphere of 5% CO_2 and 95% air at 37 °C humidified air till 70–80% confluency.

Cell Imaging Study. For confocal imaging studies, RAW cells, 1×10^{-5} cells in 150 μL of medium, were seeded on sterile 12 mm diameter Poly L lysine coated coverslip, kept in a sterile 35 mm covered Petri dish, and incubated at 37 °C in a CO_2 incubator for 24–30 h. The next day, cells were washed three times with phosphate buffered saline (pH 7.4) and fixed using 4% paraformaldehyde in PBS (pH 7.4) for 10 min at room temperature washed with PBS followed by permeabilization using 0.1% saponin for 10 min. Then the cells were incubated with 2.0×10^{-4} M $SnCl_4$ dissolved in 100 μL DMEM at 37 °C for 1 h in a CO_2 incubator and observed under Andor spinning disk confocal microscope with excitation at 561 nm monochromatic laser beam, and the collected range of emission wavelength was between 630 and 650 nm. The cells were again washed thrice with PBS (pH 7.4) to remove any free metal and incubated in DMEM containing probe to a final concentration of 1×10^{-6} M followed by washing with PBS (pH 7.4) three times to remove excess probe outside the cells. Again, images were captured using EMCCD camera. In a separate coverslip undergoing the same treatment the cells were then treated with 30 μM of Na_2S solution for 1 h; the cells

dx.doi.org/10.1021/ic4007026 | Inorg. Chem. 2013, 52, 10825–10834

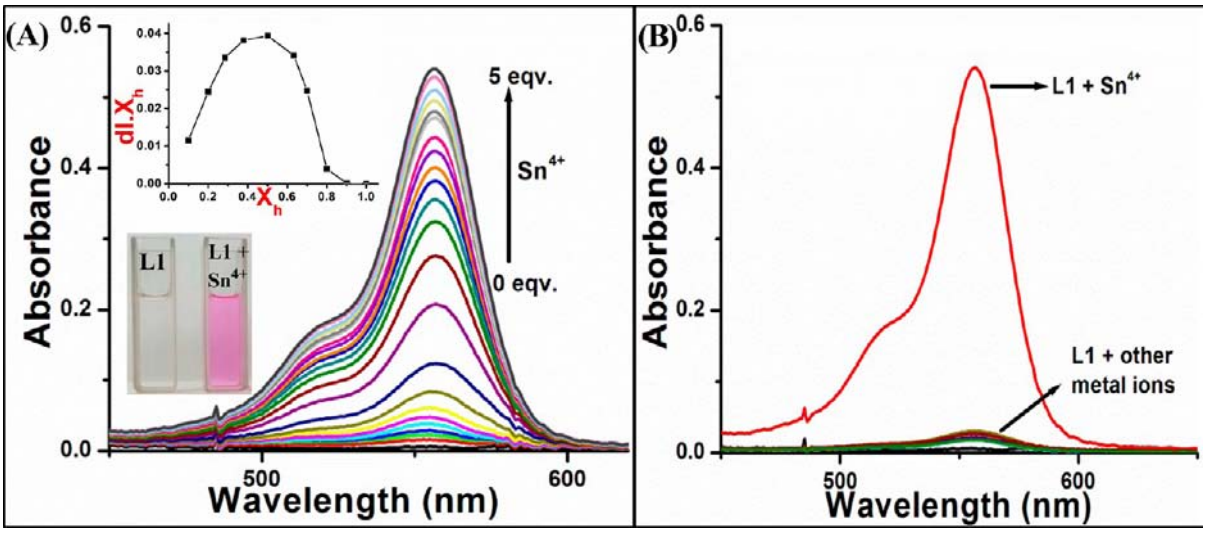

Figure 1. (A) UV−vis absorption titration spectra of spectra of **L1** ($c = 4\times 10^{-5}$ M) in aq CH_3OH (CH_3OH/H_2O = 4:1, v/v, 10 μM HEPES buffer, pH = 7.4) upon addition of Sn^{4+} ($c = 2\times 10^{-4}$ M). Inset: Job's plot that indicates 1:1 stoichiometry and photographs of **L1** and **L1** + Sn^{4+}. (B) Competitive absorption spectra of **L1** in the presence of different metal ions (perchlorate, chloride, or nitrate salts of Cr^{3+}, Mg^{2+}, Ca^{2+}, Al^{3+}, Mn^{2+}, Fe^{2+}, Fe^{3+}, Co^{2+}, Ni^{2+}, Cu^{2+}, Zn^{2+}, Cd^{2+}, Hg^{2+}, Ag^{+}, and Pb^{2+}) in aq CH_3OH (CH_3OH/H_2O = 4:1, v/v, 10 μM HEPES buffer, pH = 7.4).

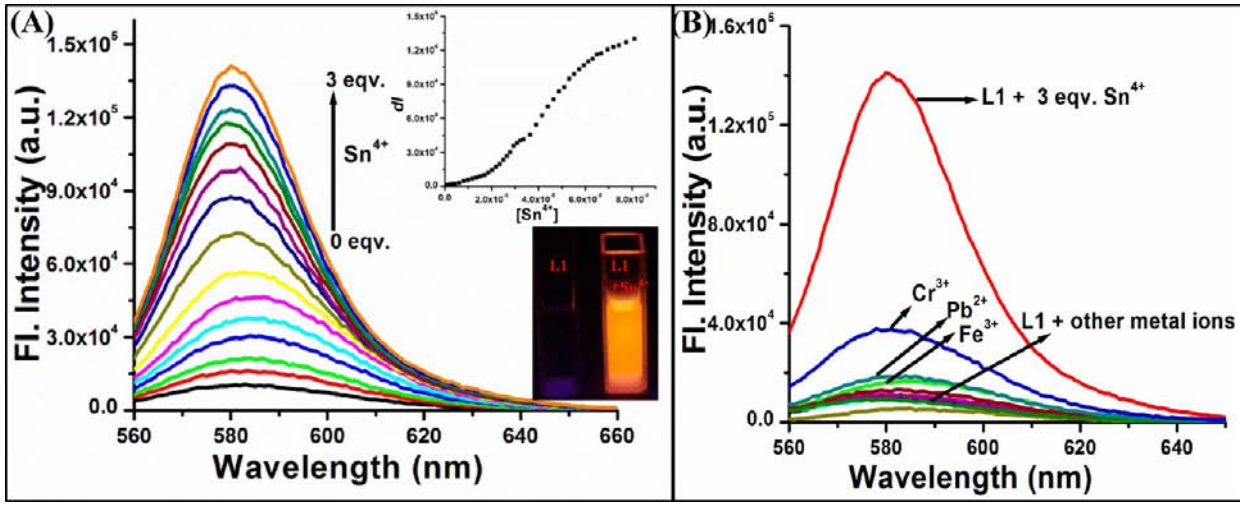

Figure 2. (A) Fluorescence emission spectra of **L1** ($c = 4\times 10^{-5}$ M) in aq CH_3OH (CH_3OH/H_2O = 4:1, v/v, 10 μM HEPES buffer, pH = 7.4) upon addition of Sn^{4+} ($c = 2\times 10^{-4}$ M). Inset: Change of emission intensity at 580 nm with incremental addition of Sn^{4+} (λ_{ext} = 555 nm) and fluorescence photographs of **L1** and **L1** + Sn^{4+}. (B) Competitive fluorescence spectra of **L1** in the presence of different metal ions (perchlorate, chloride, or nitrate salts of Cr^{3+}, Mg^{2+}, Ca^{2+}, Al^{3+}, Mn^{2+}, Fe^{2+}, Fe^{3+}, Co^{2+}, Ni^{2+}, Cu^{2+}, Zn^{2+}, Cd^{2+}, Hg^{2+}, Ag^{+}, and Pb^{2+}) in aq CH_3OH (CH_3OH/H_2O = 4/1, v/v, 10 μM HEPES buffer, pH = 7.4).

were washed with PBS three times to remove free compound and ions before analysis. Before microscopic imaging, all the solutions were aspirated and mounted on slides in a mounting medium containing DAPI (1 μg/mL) and stored in dark before microscopic images are acquired.

Cytotoxic Effect on Cells. The cytotoxic effects of probe **L1**, $SnCl_4$, and **L1**−$SnCl_4$ complex were determined by an MTT assay following the manufacturer's instruction (MTT 2003, Sigma-Aldrich, MO). HCT cells were cultured into 96-well plates (approximately 10^4 cells per well) for 24 h. The next day, the medium was removed, and various concentrations of **L1**, $SnCl_4$, and **L1**−$SnCl_4$ complex (0, 15, 25, 50, 75, and 100 μM) made in DMEM were added to the cells and incubated for 24 h. Solvent control samples (cells treated with DMSO in DMEM), no cells, and cells in DMEM without any treatment were also included in the study. Following incubation, the growth medium was removed, and fresh DMEM containing MTT solution was added. The plate was incubated for 3−4 h at 37 °C. Subsequently, the supernatant was removed, the insoluble colored formazan product was solubilized in DMSO, and its absorbance was measured in a microtiter plate reader (Perkin-Elmer) at 570 nm. The assay was performed in triplicate for each concentration of **L1**, $SnCl_4$, and **L1**−$SnCl_4$ complex. The OD value of wells containing only DMEM medium was subtracted from all readings to get rid of the background influence. Data analysis and calculation of standard deviation were performed with Microsoft Excel 2007 (Microsoft Corporation).

Computational Studies. All geometries for **L1** and **L1**·Sn^{4+} were optimized by density functional theory (DFT) calculations using Gaussian 2003(B3LYP/6-31G(d,p)) software package.[22]

RESULTS AND DISCUSSION

UV−Vis Spectroscopic Studies of L1 in Presence of Sn^{4+}. The absorption spectra of **L1** with Sn^{4+} was investigated by spectrophotometric titration in CH_3OH/aqueous HEPES buffer (1 mM, pH 7.4; 4:1, v/v). When no Sn^{4+} ions were added to the solution of **L1**, free **L1**, as expected, exhibited

dx.doi.org/10.1021/ic4007026 | Inorg. Chem. 2013, 52, 10825−10834

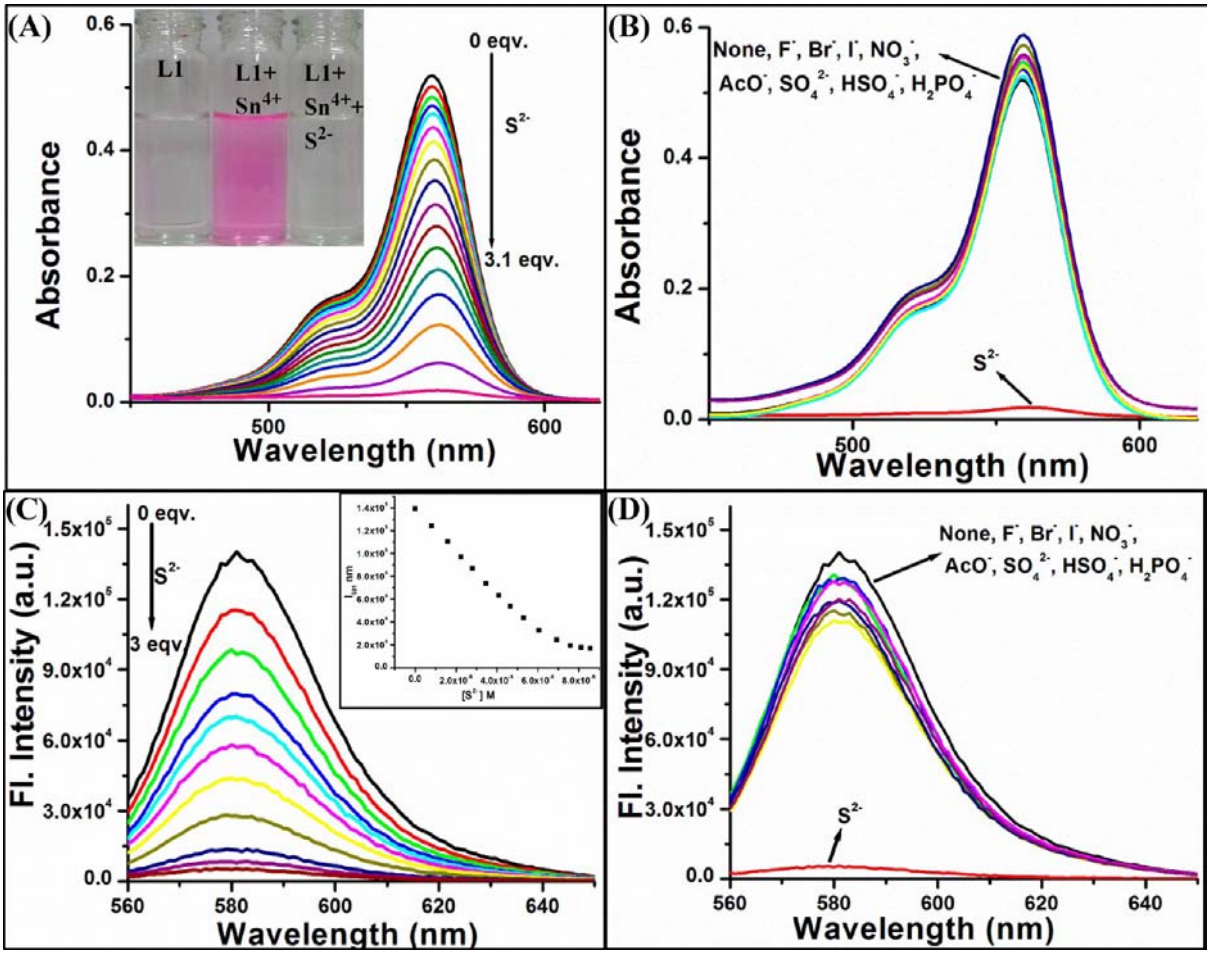

Figure 3. (A) UV−vis titration spectra of **L1** ($c = 4\times 10^{-5}$ M) with 3 equiv of Sn^{4+} upon addition of sodium sulfide ($c = 2\times 10^{-4}$ M) in aq CH_3OH (CH_3OH/H_2O = 4:1, v/v, 10 μM HEPES buffer, pH = 7.4). Inset: Photographs of **L1**, **L1** + Sn^{4+}, **L1** + Sn^{4+}, + S^{2-} in color changes. (B) Changes in the absorption spectra of **L1**−Sn complex in presence of different anions. (C) Fluorescence spectra of **L1** ($c = 4\times 10^{-5}$ M) with 3 equiv of Sn^{4+} upon addition of sodium sulfide ($c = 2 \times 10^{-4}$ M) in aq CH_3OH (CH_3OH/H_2O = 4:1, v/v, 10 μM HEPES buffer, pH = 7.4) Inset: Change in the fluorescence intensity at 580 nm with incremental addition of Sn^{4+} (λ_{ext} = 555 nm). (D) Changes in the fluorescence spectra of **L1**−Sn complex in presence of different anions.

almost no absorption in the visible region, indicating that **L1** exists as a spirocyclic form. It can be seen from Figure 1A that the solution of **L1** exhibits almost no absorption peak in the visible region. However, upon addition of Sn^{4+} ion, a new absorption band at 555 nm appeared with a shoulder at 518 nm, and absorbance increased with increasing Sn^{4+} concentration (0−5 equiv of Sn^{4+}), which can be ascribed to the formation of the ring-opened amide form of **L1** upon Sn^{4+} ion binding.

Meanwhile, the titration solution turned pink instantaneously as a result of the ring-open structure formation caused by Sn^{4+} binding (Figure 1A, inset), suggesting that chemosensor **L1** can serve as a "naked-eye" indicator for Sn^{4+} ions. The binding ability of **L1** was checked with perchlorate, chloride, and nitrate salts of Cr^{3+}, Mg^{2+}, Ca^{2+}, Al^{3+}, Mn^{2+}, Fe^{2+}, Fe^{3+},Co^{2+}, Ni^{2+}, Cu^{2+}, Zn^{2+}, Cd^{2+}, Hg^{2+}, Ag^{+}, and Pb^{2+} ions in CH_3OH/aqueous HEPES buffer (1 mM, pH 7.4; 4:1, v/v). A significant change in electronic spectral pattern was observed only in the presence of Sn^{4+}, among all the metal ions used (Figure 1B). The absorbance peak was no longer changed when the concentration of Sn^{4+} increased from 5 to 6 equiv, implicating a 1:1 complexation of the ligand with the Sn^{4+} ion. From the Job's plot, we can observe that the absorbance went through a maximum at a molar fraction of about 0.5, indicating that a 1:1 stoichiometry was most possible for the binding mode of Sn^{4+} and **L1** (Figure 1A, inset).

Fluorescence Spectroscopic Studies of L1 in Presence of Sn^{4+}. Fluorescence titrations of chemosensor **L1** with Sn^{4+} in CH_3OH/aqueous HEPES buffer (1 mM, pH 7.4; 4:1, v/v) were performed. The fluorescence spectra were obtained by excitation at 555 nm. As shown in Figure 2A, free probe **L1** showed almost no fluorescence due to the spirocyclic structure. However, the treatment with Sn^{4+} induced a dramatic change at 580 nm in the fluorescence spectra (14-fold) which was higher than the result obtained with the rhodamine-based Sn^{4+} sensors reported earlier.[23] Upon addition of Sn^{4+}, the fluorescence intensity increased in a Sn^{4+} concentration-dependent way as shown in Figure 2A (inset), accompanied with an obvious orange fluorescence enhancement . The results indicated that the spirolactam ring was opened and conjugated structure was formed. The recognition interaction was completed immediately after the addition of Sn^{4+} within 1 min, and hence, **L1** could be used in real-time determination of Sn^{4+} in environmental and biological conditions. There was a significant emission intensity enhancement (14-fold) with 3.0 equiv of

dx.doi.org/10.1021/ic4007026 | Inorg. Chem. 2013, 52, 10825−10834

Scheme 2. Proposed Mechanism for the Fluorescence Changes of L1 upon Addition of Sn^{4+}

Sn^{4+} which indicates that compound **L1** is an excellent turn-on sensor for Sn^{4+}.

From the emission titration experiment, the association constant[24] (K_a) of **L1** with Sn^{4+} was estimated to be 4.31×10^4 M^{-1} (Figure S9, Supporting Information). The detection limit of Sn^{4+} is about 2.58 μM (Supporting Information). The selectivity of **L1** to the various metal ions were investigated. On addition of different metal ions, *viz.*, Cr^{3+}, Mg^{2+}, Ca^{2+}, Al^{3+}, Mn^{2+}, Fe^{2+}, Fe^{3+}, Co^{2+}, Ni^{2+}, Cu^{2+}, Zn^{2+}, Cd^{2+}, Hg^{2+}, Ag^{+}, and Pb^{2+}, to solution of **L1**, there is no significant change in its fluorescence spectrum except in the case of addition of Sn^{4+} ions. As shown in Figure 2A, only the addition of Sn^{4+} resulted in a prominent enhancement of fluorescence at 580 nm (absorbance at 555 nm), which obviously implied the high selectivity of **L1** to Sn^{4+}. The competition experiments (Figure 2B), which were carried out by adding Sn^{4+} to **L1** solution in the presence of other metal ions, revealed that there was no significant interference of Sn^{4+}-induced fluorescent responses by the commonly coexistent metal ions (Figure S6, Supporting Information).

Interestingly, a solution of **L1** in optimized CH_3OH/H_2O solution (4:1, v/v, HEPES buffer, pH = 7.2) is colorless and emits no orange fluorescent light, but during the fluorometric titration of **L1** with Sn^{4+} ions the colorless solution of the receptor became deep orange (Figure 2A, inset). This orange fluorescent color is attributed to the opening of the spirolactam ring and generation of the delocalized xanthene moiety,[25] whereas compound **L1** shows obvious pink color in buffered CH_3OH/HEPES solution upon addition of Sn^{4+} under visible light. This was not observed with other metal ions (Figure S8, Supporting Information). The results support our expectation that **L1** could serve as a sensitive naked-eye probe for Sn^{4+}.

Selective Optical Response of L1−Sn Complex to Various Anions. Hence, from the UV−vis and fluorescence studies we can conclude that **L1** selectively binds with Sn^{4+} to form **L1**−Sn complex with considerable change in its spectral properties. An important property of the chemosensor is high selectivity toward the analyte as well as the reversibility in the complexation of any probe to be employed as a chemical sensor for detection of specific metal ions. Therefore, we have further studied the influence of different anions on the rupture of this metal−ligand complex and their effect on the reversibility of **L1**−Sn complex to regenerate **L1**. It is very exciting and noteworthy that compound **L1** could be regenerated only by adding S^{2-} to the solution containing **L1**−Sn. Commom anions, such as F^-, Br^-, I^-, NO_3^-, SO_4^{2-}, CH_3COO^-, HSO_4^-, and $H_2PO_4^-$, and other forms of sulfate, did not generate the same results. Addition of Na_2S to the solution of complex of **L1**−Sn brought the reverse change in the absorption spectra (Figure 3A).

A similar finding was observed in emission (Figure 3C). The **L1**−Sn system revealed remarkably selective fluorescence "off" behavior exclusively with S^{2-}. As shown in Figure 3C, upon the addition of various amounts of sulfide ions (0−3 equiv) in the presence of 3 equiv of Sn^{4+}, both the intensity and shape of the system's emission spectrum return to those of the native **L1** state. Figure 3C shows that the intensity of the fluorescence emission decreases with increasing concentration of sulfide anion, and on addition of nearly about 3 equiv of S^{2-} anion both the intensity and overall pattern of emission spectrum closely match those of compound **L1** (Figure 2A), so the fluorescence intensity along with the maximum emission peak are totally regenerated. However, there were nearly no differences in the presence and absence of other anions (Figure 3B,D). This showed that Sn^{4+} was released from complex **L1**−Sn, and SnS_2 formed. The calibration curve of the fluorescence intensity at 580 nm of **L1** (Figure 3C, inset) elucidated that sulfide anion interacted with Sn^{4+}. For further understanding, we carried out UV−vis titration in this complex. On addition of the aqueous solution of Na_2S to the deep pink solution of **L1**−Sn, spectral bands (absorption band with λ_{max} at 555 nm), as well as the color of the solution, disappeared (Figure 3A, inset). Again, on addition of Sn^{4+} to this solution mixture having Na_2S, the absorbance band at 555 nm and emission band at 580 nm reappeared (Figure S11, Supporting Information). Simultaneously, the pink color of the solution was also restored.

Preferential binding of the S^{2-} ion to the Sn^{4+} ion led to the formation of SnS_2 and the regeneration of the cyclic lactam form of the reagent, a process which is well documented for demonstrating the reversible binding of rhodamine derivatives to Sn^{4+}. This signifies that signal transduction is reversible; therefore, the chemosensor would be recyclable (Figure S11, Supporting Information), which is a highly efficient one. Reversible binding of Sn^{4+} to **L1** was also established through spectral studies in presence of 3 equiv of Na_2EDTA (Figure S10, Supporting Information).

Sensing Mechanism. In order to gain insight into the sensing mechanism, we decided to study the sensing process by

dx.doi.org/10.1021/ic4007026 | *Inorg. Chem.* 2013, 52, 10825−10834

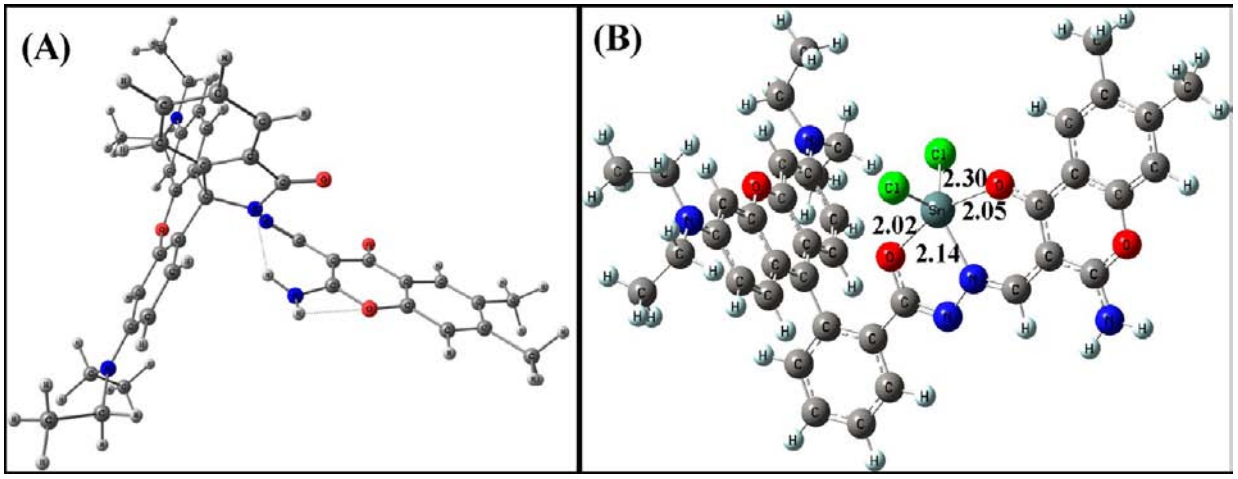

Figure 4. Calculated energy-minimized structure of (A) **L1** and (B) **L1**−Sn complex.

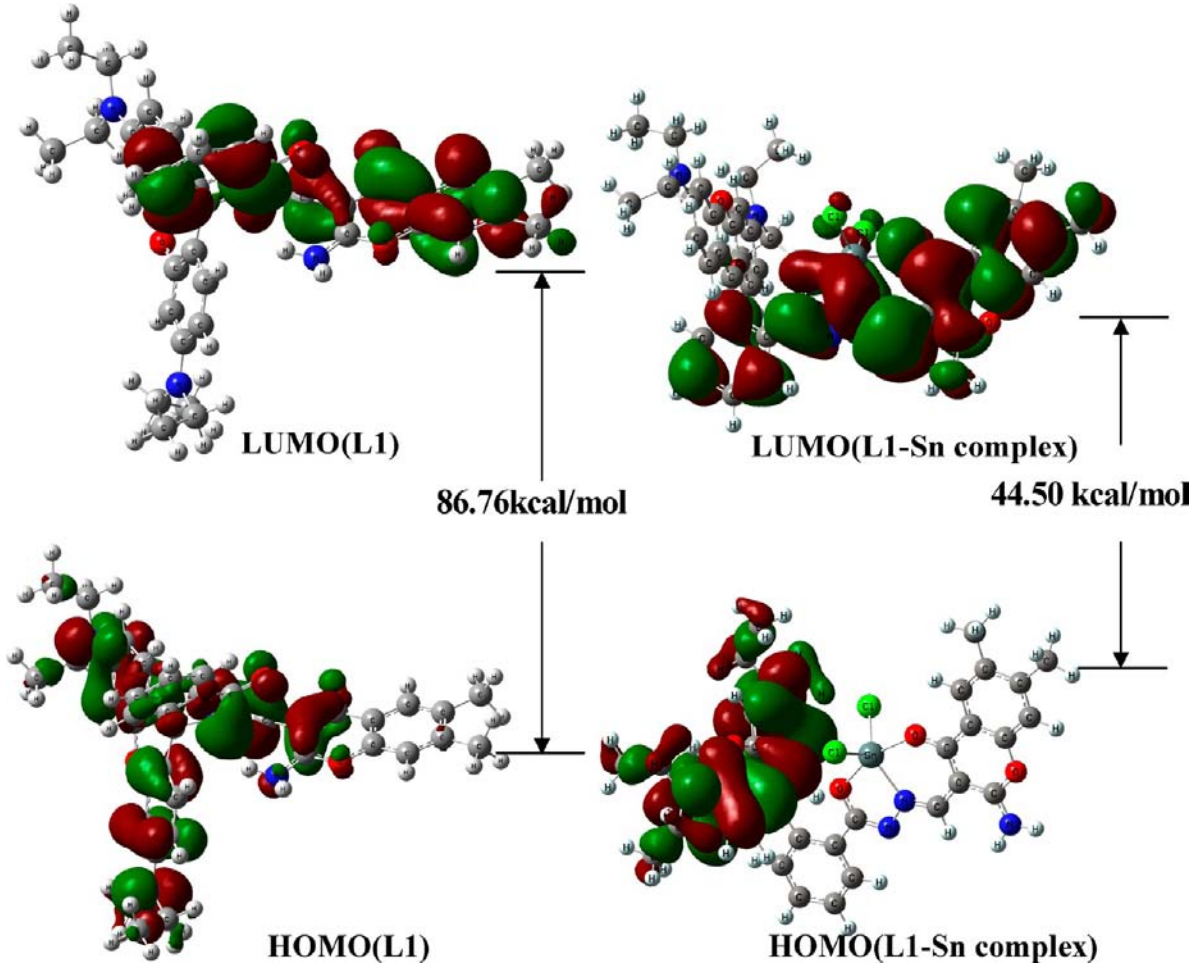

Figure 5. HOMO and LUMO distributions of **L1** and **L1**−Sn^{4+} complex.

FTIR, HRMS, and the density functional theory (DFT) calculation. The complex formed between **L1** and Sn^{4+} is found to be 1:1 in stoichiometry, which is confirmed from the Job's plot for binding of Sn^{4+} to **L1** by UV−vis spectrometry. The result was also confirmed through HRMS analysis, and it is well matched with theoretical mass spectral simulation. The peak at m/z 844.0773 in the mass spectrum is assignable to the mass of $[(\mathbf{L1} + Sn^{4+} + 2Cl^{-} - 1)^{+}]$ (Figure S4, Supporting Information). The role of the C═O amide bond on binding Sn^{4+} cations was examined using FTIR techniques. FTIR spectra of **L1** revealed that the peak at 1682 cm^{-1}, the characteristic stretching frequency for the CO amide bond of the rhodamine unit, shifted to 1634 cm^{-1} in presence of 1.5 equiv of the Sn^{4+} ion (Figure S12, Supporting Information). Such a shift in the stretching frequency of C═O amide bond of the rhodamine unit on binding to a metal ion has been reported

dx.doi.org/10.1021/ic4007026 | *Inorg. Chem.* 2013, 52, 10825−10834

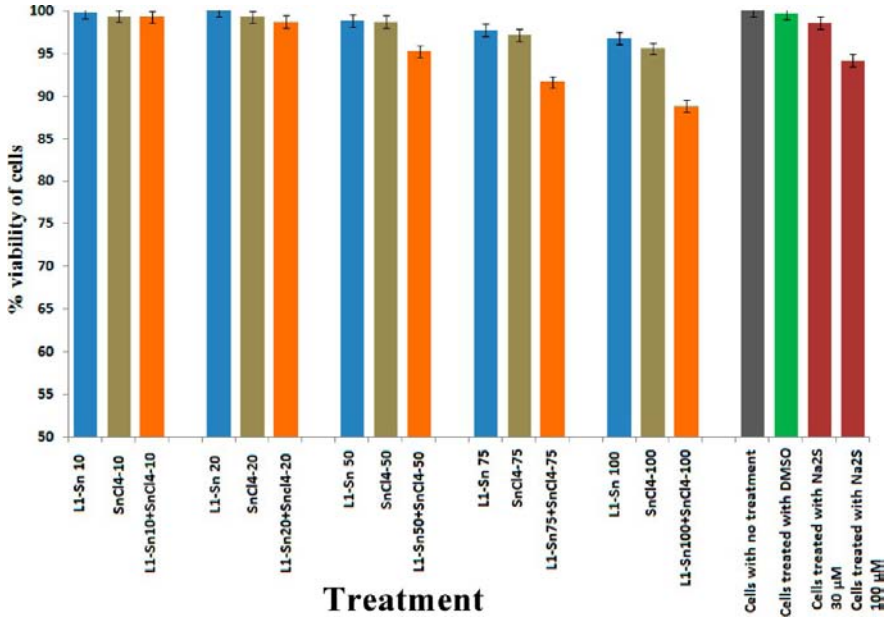

Figure 6. MTT assay to determine the cytotoxic effect of **L1** and **L1**−Sn complex on HCT cells.

earlier.[26] Thus, FTIR studies suggest that the shift in the stretching frequency of C═O bond was due to its participation in the binding event of the metal cation. Furthermore, in order to investigate the "on−off" property, the HRMS spectrum of the [**L1** + Sn^{4+} + S^{2-}] system was obtained also. The parent peak [M + Na^+]$^+$ at m/z 678.2179 (Figure S5, Supporting Information) is equivalent to that of compound **L1** on addition of S^{2-}. Therefore, it elucidated the mechanism of the sensing of sulfide anions. From our Sn^{4+} binding studies it was also evident that the binding induced breakage of the spirolactum ring of **L1** initiates the turn on fluorescence. As illustrated in Scheme 2, the addition of Sn^{4+} ion can cause fluorescence on (Φ = 0.132), simultaneously inducing a color change from colorless to deep pink. Also, the added sulfide can capture Sn^{4+} ion, resulting in fluorescence quenching (Φ = 0.061) and inducing a deep pink to colorless colorimetric change (Figure 3A, inset). This fluorescence enhancement can be attributed to complex **L1**−Sn formation upon the addition of Sn^{4+}, as shown in Scheme 2, and then the tin ions were captured by sulfide ions, resulting in the revival of **L1**, which is accompanied by fluorescence off and disappear of color. Therefore, the above-mentioned fact provides strong evidence of the dissociation of **L1**−Sn complex in the presence of S^{2-} anions to restore the native structure of **L1**.

Density Functional Theory (DFT) Calculations. As the stoichiometry of the complex formed between **L1** and Sn^{4+} was found to be 1:1 on the basis of emission, absorption, and HRMS studies, for better understanding, the nature of Sn^{4+} coordination with **L1** was studied by computational studies using the Gaussian 2003(B3LYP/6-31G(d,p)) software package.[22] The geometry optimizations for **L1** and **L1**−Sn complex were done in a cascade fashion starting from semiempirical PM2 followed by *ab initio* HF to DFT B3LYP by using various basis sets, *viz.*, PM2 → HF/STO-3G → HF/3-21G → HF/6-31G → B3LYP/6-31G(d,p). For **L1**−Sn complex, a starting model was generated by taking the DFT optimized **L1** and placing the Sn^{4+} ion well in the core of the imidecarbonyl O, enamine N, benzopyrancarbonyl O, and/benzopyranamine N as donor moieties at a noninteracting distance. This model was then optimized initially using HF/3-21G level of calculations, and the output structure from this was taken as input for DFT calculations performed using B3LYP with SDDAll basis set for Sn^{4+} and 6-31+G(d,p) for all other atoms in the complex.

The spatial distributions and orbital energies of HOMO and LUMO of **L1** and **L1**−Sn were also determined (Figure 5). The π electrons on the HOMO of **L1**−Sn complex are mainly located on the imidecarbonyl of rhodamine part and unsaturated carbonyl of benzopyran framework, but the LUMO is mostly positioned at the center of the guest Sn^{4+} ion. Moreover, the HOMO−LUMO energy gap of the complex becomes much smaller relative to that of probe **L1**.

The energy gaps between HOMO and LUMO in the probe **L1** and **L1**−Sn complex were 86.76 and 44.50 kcal mol^{-1}, respectively (Supporting Information). The results clearly suggest that the Sn^{4+} ion binds to **L1** very well through five coordination sites, and the whole molecular system forms a nearly planar structure. The optimized complex of Sn^{4+} with **L1** (Figure 5) showed that a distinct low energy complexation occurs between Sn^{4+} and benzopyrancarbonyl O sites of oxo-chromene due to resonance effect of NH_2 and the ring oxygen atom (Table S1, Supporting Information). Hence, the interaction of the benzopyrancarbonyl O atom with Sn^{4+} can change the orbital energy level, realizing the optical detection. The optimized complex of Sn^{4+} with **L1** at this stage showed a nearly planar pentacoordinated geometry around Sn^{4+} where all five bonds (2 × Sn−O, Sn−N, and 2 × Sn−Cl) are bonded to the central ion with their distances of 2.02, 2.05, 2.14, and 2.30 Å, respectively (Figure 4B).

These Sn−O, Sn−Cl, and Sn−N distances are comparable with the experimental ones reported in the literature for pentacoordinate Sn(IV) complexes.[27]

To study the practical applicability, the effects of pH on the fluorescence response of **L1** in the absence and presence of Sn^{4+} ions were evaluated. In the absence of Sn^{4+}, almost no change in fluorescence intensity was observed in the free sensor over a wide pH range of 5.5−11.0, indicating that the free sensor **L1** was stable in the wide pH range. Experimental results show that, for free **L1**, at acidic conditions (pH < 5), an obvious

dx.doi.org/10.1021/ic4007026 | *Inorg. Chem.* 2013, 52, 10825−10834

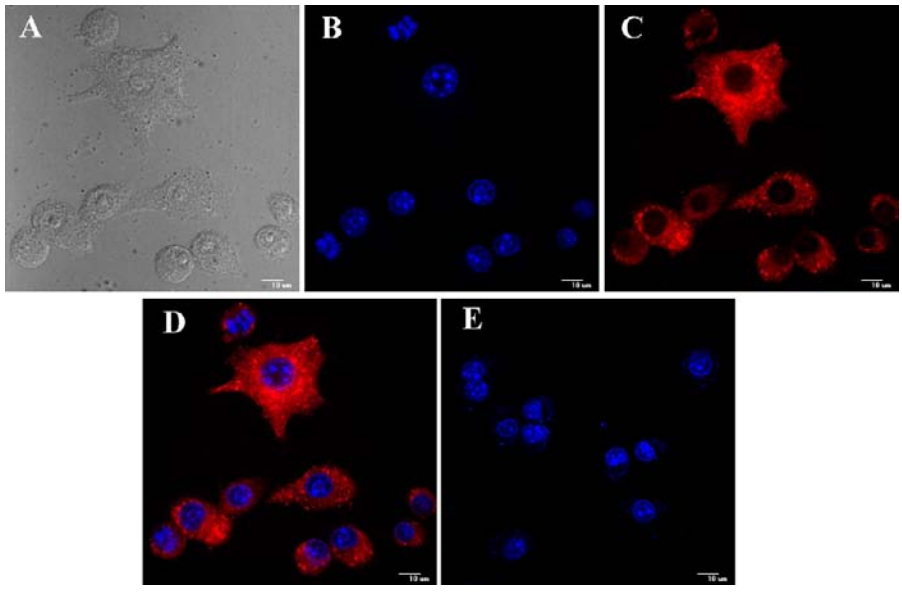

Figure 7. Confocal microscopic images of probe in RAW 264.7 cells pretreated with $SnCl_4$: (A) bright field image of the cells, (B) only $SnCl_4$ at 2.0×10^{-4} M concentration, nuclei counterstained with DAPI (1 μg/mL), (C) stained with probe **L1** at concentration 1.1×10^{-6} M, (D) overlay image in dark field, (E) and cells treated with $SnCl_4$ at 2.0×10^{-4} M, probe at concentration 1.1×10^{-6} M and Na_2S (30 μM), no red signal is detected . All images were acquired with a 40× objective lens.

off−on fluorescence appeared due to the formation of the open-ring state because of the strong protonation. In the pH range from 4.0 to 6.0, little fluorescence signal (excited at 555 nm) could be observed for free **L1**, suggesting that the molecules prefer the spirocyclic form. Upon the addition of Sn^{4+} ions, there was an obvious fluorescence off−on change of **L1** under different pH values. Thus, the sensor **L1** has the maximal sensing response at physiological pH, indicating that the sensor **L1** is promising for biological applications (Figure S7, Supporting Information).

Biological Studies of L1 in Presence of Sn^{4+} and S^{2-}. Due to its favorable binding properties with Sn^{4+} and its complex **L1**−Sn showing intense emission in visible region, practical bioimaging application of the probe **L1** could be exploited for sensitive detection of intracellular tin. However, to materialize this objective it is a prerequisite to assess the cytotoxic effect of probe **L1**, Sn^{4+}, and the complex on live cells. The well-established MTT assay, which is based on mitochondrial dehydrogenase activity of viable cells, was adopted to study cytotoxicity of the above-mentioned compounds at varying concentrations mentioned in the Experimental Section. Figure 6 shows that probe **L1** did not exert any adverse effect on cell viability, and the same is the case when cells were treated with varying concentrations of Sn^{4+}. However, exposure of HCT cells to **L1**−Sn complex resulted in a decline in cell viability above 20 μM concentration. The effect was more pronounced in higher concentration and showed an adverse cytotoxic effect in a dose-dependent manner which is in agreement with previous literature reports suggesting cytotoxic and antiproliferative effects of **L1**−Sn complex on cancer cells.[28]

The viability of HCT cells was not influenced by the solvent (DMSO) as evidenced in Figure 6, leading to the conclusion that the observed cytotoxic effect could be attributed to **L1**−Sn complex. Also, Na_2S does not significantly affect the cell viability either, even in 100 μM (Figure 6), and thus, the probe can also detect sulfide in biological systems.

The results obtained in the in vitro cytotoxic assay suggested that, in order to pursue confocal imaging studies of **L1**−Sn complex in live cells, it would be prudent to choose a working concentration of 20 μM for probe compound. Hence, to assess the effectiveness of compound **L1** as a probe for intracellular detection of Sn^{4+} by confocal microscopy, RAW cells were treated with 20 μM $SnCl_4$ for 1 h followed by 10 μM probe solution to promote formation of **L1**−Sn complex. Confocal microscopic studies revealed a lack of fluorescence for RAW cells when treated with either probe compound or $SnCl_4$ alone (Figure 7B). Upon incubation with $SnCl_4$ followed by probe **L1**, a striking switch-on fluorescence was observed inside RAW cells, which indicated the formation of **L1**−Sn complex, as observed earlier in solution studies. Further, an intense red fluorescence was conspicuous in the perinuclear region of RAW cells (Figure 7C).

Interestingly, when the cells were treated with Na_2S solution (Figure 7E) this bright red fluorescence was significantly gone. Sulfide sensing inside RAW cells by **L1**−$SnCl_4$ complex could also be pursued as evident from this remarkable switch-off of the red fluorescence emission inside cells following incubation with Na_2S solution.

The confocal microscopic analysis strongly suggested that probe **L1** could readily cross the membrane barrier of the RAW cells, and rapidly sense intracellular Sn^{4+} and S^{2-}. It is significant to mention here that bright field images of treated cells did not reveal any gross morphological changes, which suggested that RAW cells were viable. These findings open up the avenue for future in vivo biomedical applications of the sensor.

CONCLUSION

A structurally characterized oxo-chromene rhodamine B derivative of **L1** exhibits high selectivity toward Sn^{4+}. The selectivity has been demonstrated by fluorescence, absorption, and HRMS spectroscopy. Interaction of Sn^{4+} with **L1** enhances the fluorescence emission at 580 nm and induces a turn-on

dx.doi.org/10.1021/ic4007026 | Inorg. Chem. 2013, 52, 10825−10834

response in electronic and fluorescence spectra in the visible region. **L1** is sensitive and selective toward Sn^{4+} over other biologically important ions studied, *viz.*, Cr^{3+}, Mg^{2+}, Ca^{2+}, Al^{3+}, Mn^{2+}, Fe^{2+}, Fe^{3+}, Co^{2+}, Ni^{2+}, Cu^{2+}, Zn^{2+}, Cd^{2+}, Hg^{2+}, Ag^{+}, and Pb^{2+}, as demonstrated by individual as well as competitive metal ion titrations. Thus, these receptors could be used as a dual probe for visual detection through change in color and fluorescence. Whereas the fluorescence and absorption spectroscopy provided information for the formation of 1:1 complex between $Sn^{4+}$and **L1**, *viz.*, **L1**−Sn, the HRMS confirmed the same unambiguously by exhibiting correct peak pattern for the presence of tin in the complex. The tin-binding capabilities of the nitrogen−oxygen binding core of oxo-chromene rhodamine moieties available in **L1** has been examined by computational calculations at the DFT level. The theoretical studies supported that Sn^{4+} coordinating with the O atom of the oxo-chromene moiety, accompanied by the transferring of electrons of the oxo-chromene, resulted in the opening of the spiro-ring. The *in situ* prepared tin complex of **L1**, *viz.*, **L1**−Sn, was able to detect S^{2-} in exactly the reverse manner compared to what happens when Sn^{4+} is added to **L1** in fluorescence spectroscopy. Thus, upon addition of S^{2-} to **L1**−Sn, the 580 nm band intensity decreases, suggesting the release of **L1** from the tin complex. The receptor **L1** shows intense change in its fluorescence emission when bound to Sn^{4+} in physiological conditions. Hence, the effectiveness of compound **L1** as a probe for intracellular detection of Sn^{4+} by confocal microscopy was also studied. Moreover, the confocal microscopic analysis strongly suggested that compound **L1** could readily cross the membrane barrier of the RAW cells, and rapidly sense intracellular Sn^{4+} and S^{2-}.

■ ASSOCIATED CONTENT

Supporting Information

^{1}H NMR, ^{13}C NMR, mass, and IR spectra as characterization data of **L1** and **L1**−Sn complex. Benesi−Hildebrand plot, Job's plot, UV−vis spectra, and photograph of the **L1** solution in presence and absence of Sn^{4+} ions. Additional tables. This material is available free of charge via the Internet at http://pubs.acs.org.

■ AUTHOR INFORMATION

Corresponding Author

*E-mail: mahapatra574@gmail.com. Fax: +91 33 26684564. Phone: +91 33 2668 4561.

Author Contributions

The manuscript was written through contributions of all authors. All authors have given approval to the final version of the manuscript.

Notes

The authors declare no competing financial interest.

■ ACKNOWLEDGMENTS

We thank the DST-New Delhi (Project SR/S1/OC-44/2012) for financial support. S.K.M. thanks UGC, New Delhi, India, for a fellowship and also Bhaskar Pramanik for his support. We are also thankful to Annesur Rahaman Centre for High Performance Computing, IACS, Kolkata, for providing us with computational time.

■ REFERENCES

(1) (a) Chen, T.; Zhu, W.; Xu, Y.; Zhang, S.; Zhang, X.; Qian, X. *Dalton Trans.* **2010**, *39*, 1316−1320. (b) Ho, M.-L.; Chen, K.-Y.; Lee, G.-H.; Chen, Y.-C.; Wang, C.-C.; Lee, J.-F. *Inorg. Chem.* **2009**, *48*, 10304−10311. (c) Huang, W.; Zhou, P.; Yan, W.; He, C.; Xiong, L.; Li, F.; Duan, C. *J. Environ. Monit.* **2009**, *11*, 330−335.

(2) (a) Snoeij, N. J.; Penninks, A. H.; Seinen, W. *Environ. Res.* **1987**, *44*, 335−353. (b) Sherman, L. R.; Masters, J.; Peterson, R.; Levine, S. *J. Anal. Toxicol.* **1986**, *10*, 6−9.

(3) (a) Florea, A.-M.; Büsselber, D. *BioMetals* **2006**, *19*, 419−427. (b) *Concise International Chemical Assessment Document 65*; WHO: Geneva, 2006.

(4) (a) Kim, H. N.; Guo, Z.; Zhu, W.; Yoon, J.; Tian, H. *Chem. Soc. Rev.* **2011**, *40*, 79−93. (b) Boens, N.; Leen, V.; Dehaen, W. *Chem. Soc. Rev.* **2012**, *41*, 1130−1172. (c) Xu, Z.; Han, S. J.; Lee, C.; Yoon, J.; Spring, D. R. *Chem. Commun.* **2010**, *46*, 1679−1681.

(5) Haugland, R. P. Molecular Probes. *The Handbook: A Guide to Fluorescent Probes and Labeling Technologies*, 10th ed.; Invitrogen Corporation: Carlsbad, CA, 2005.

(6) Yang, H.; Zhou, Z.; Huang, K.; Yu, M.; Li, F.; T, Yi.; Huang, C. *Org. Lett.* **2007**, *9*, 4729−4732.

(7) Lakowicz, J. R. *Principles of Fluorescence Spectroscopy*, 3rd ed.; Springer: New York, 2006; p 67.

(8) Yang, Y.-K.; Shim, S.; Tae, J. *Chem. Commun.* **2010**, *46*, 7766−7768.

(9) (a) Zhaoa, Y.; Zhenga, B.; Dua, J.; Xiao, D.; Yanga, L. *Talanta* **2011**, *85*, 2194−2201. (b) Zhou, Y.; Zhang, J.; Zhou, H.; Zhang, Q.; Ma, T.; Niu, J. *Sens. Actuators, B* **2012**, *171*−*172*, 508−514. (c) Mahapatra, A. K.; Manna, S. K.; Mukhopadhyay, S. K.; Banik, A. *Sens. Actuators, B* **2013**, *183*, 350−355. (d) Qi, W.; Li, C.; Zou, Y.; Wang, H.; Yi, T.; Huang, C. *Org. Biomol. Chem.* **2012**, *10*, 6740−6746.

(10) (a) Kumar, M.; Kumar, N.; Bhalla, V.; Sharma, P. R.; Kaur, T. *Org. Lett.* **2012**, *14*, 406−409. (b) Kar, C.; Adhikari, M. D.; Ramesh, A.; Das, G. *Inorg. Chem.* **2013**, *52*, 743−752.

(11) (a) Weerasinghe, A. J.; Schmiesing, C.; Sinn, E. *Tetrahedron Lett.* **2009**, *50*, 6407−6410. (b) Saha, S.; Mahato, P.; Reddy, G. U.; Suresh, E.; Chakrabarty, A.; Baidya, M.; Ghosh, S. K.; Das, A. *Inorg. Chem.* **2012**, *51*, 336−345.

(12) Yang, Z.; She, M.; Yin, B.; Cui, J.; Zhang, Y.; Sun, W.; Li, J.; Shi, Z. *J. Org. Chem.* **2012**, *77*, 1143−1147.

(13) Ghosh, K.; Sarkar, T.; Samadder, A. *Org. Biomol. Chem.* **2012**, *10*, 3236−3243.

(14) Kwon, J. Y.; Jang, Y. J.; Lee, Y. J.; Kim, K. M.; Seo, M. S.; Nam, W.; Yoon, J. *J. Am. Chem. Soc.* **2005**, *127*, 10107−10111.

(15) Sreenath, K.; Clark, R. J.; Zhu, L. *J. Org. Chem.* **2012**, *77*, 8268−8279.

(16) Jou, M. J.; Chen, X.; Swamy, K. M. K.; Kim, H. N.; Kim, H.-J.; Lee, S.-G.; Yoon, J. *Chem. Commun.* **2009**, 7218−7220.

(17) Yuan, M.; Zhou, W.; Liu, X.; Zhu, M.; Li, J.; Yin, X.; Zheng, H.; Zuo, Z.; Ouyang, C.; Liu, H.; Li, Y.; Zhu, D. *J. Org. Chem.* **2008**, *73*, 5008−5014.

(18) (a) Lohani, C. R.; Kim, J.-M.; Chung, S.-Y.; Yoon, J.; Lee, K.-H. *Analyst* **2010**, *135*, 2079−2084. (b) Sahana, A.; Banerjee, A.; Lohar, S.; Sarkar, B.; Mukhopadhyay, S. K.; Das, D. *Inorg. Chem.* **2013**, *52*, 3627−3633.

(19) (a) Dujols, V.; Ford, F.; Czarnik, A. W. *J. Am. Chem. Soc.* **1997**, *119*, 7386−7387. (b) Xiang, Y.; Tong, A. *Org. Lett.* **2006**, *8*, 1549−1552.

(20) (a) Benesi, H. A.; Hildebrand, J. H. *J. Am. Chem. Soc.* **1949**, *71*, 2703−2707. (b) Yang, C.; Liu, L.; Mu, T.-W.; Guo, Q.-X. *Anal. Sci.* **2000**, *16*, 537−539. (c) Shiraishi, Y.; Sumiya, S.; Kohno, Y.; Hirai, T. *J. Org. Chem.* **2008**, *73*, 8571−8574.

(21) (a) Zhu, M.; Yuan, M.; Liu, X.; Xu, J.; Lv, J.; Huang, C.; Liu, H.; Li, Y.; Wang, S.; Zhu, D. *Org. Lett.* **2008**, *10*, 1481−1484. (b) Long, L.; Zhang, D.; Li, X.; Zhang, J.; Zhang, C.; Zhou, L. *Anal. Chim. Acta* **2013**, *775*, 100−105.

(22) (a) Lee, C.; Yang, W.; Parr, R. G. *Phys. Rev. B* **1988**, *37*, 785−789. (b) Miehlich, B.; Savin, A.; Stoll, H.; Preuss, H. *Chem. Phys. Lett.* **1989**, *157*, 200−206.

(23) Liu, J.; Wu, K.; Li, X.; Han, Y.; Xia, M. *RSC Adv.* **2013**, *3*, 8924−8928.
(24) Connors, K. A. *Binding Constants—The Measurement of Molecular Complex Stability*; John Wiley & Sons: New York, 1987.
(25) (a) Saha, S.; Chhatbar, M. U.; Mahato, P.; Praveen, L.; Siddhanta, A. K.; Das, A. *Chem. Commun.* **2012**, *48*, 1659−1661. (b) Kumar, M.; Kumar, N.; Bhalla, V. *Sens. Actuators, B* **2012**, *161*, 311−316.
(26) (a) Lee, M. H.; Wu, J.-S.; Lee, J. W.; Jung, J. H.; Kim, J. S. *Org. Lett.* **2007**, *9*, 2501−2504. (b) Mahato, P.; Saha, S.; Suresh, E.; Liddo, R. D.; Parnigotto, P. P.; Conconi, M. T.; Kesharwani, M. K.; Ganguly, B.; Das, A. *Inorg. Chem.* **2012**, *51*, 1769−1777.
(27) (a) Ramírez, A.; Gomez, E.; Hernandez, S. N. *J. Organomet. Chem.* **2009**, *694*, 2965−2975. (b) Basu, S.; Gupta, G.; Das, B.; Rao, K. M. *J. Organomet. Chem.* **2010**, *695*, 2098−2104. (c) Camacho-Camacho, C.; Mijangos, E.; Castillo-Ramos, M. E.; Esparza-Ruiz, A.; Vásquez-Badillo, A.; Nöth, H.; Flores-Parra, A.; Contreras, R. *J. Organomet. Chem.* **2010**, *695*, 833−840. (d) Crawford, S. M.; Al-Sheikh Ali, A.; Cameron, T. S.; Thompson, A. *Inorg. Chem.* **2011**, *50*, 8207−821. (e) Zöller, T.; Dietz, C.; Iovkova-Berends, L.; Karsten, O.; Bradtmöller, G.; Wiegand, A.-K.; Wang, Y.; Jouikov, V.; Jurkschat, K. *Inorg. Chem.* **2012**, *51*, 1041−1056.
(28) Koch, B.; Baul, T. S. B.; Chatterjee, A. *Invest. New Drugs* **2009**, *27*, 319−326.